Lane formation in oppositely charged colloids driven by an electric field: Chaining and two-dimensional crystallization

M. Rex and H. Löwen

Institut für Theoretische Physik II: Weiche Materie, Heinrich-Heine-Universität Düsseldorf,
Universitätsstraße 1, D-40225 Düsseldorf, Germany

A binary mixture of oppositely charged colloids which is driven by an external electric field is studied by extensive Brownian dynamics computer simulations, ignoring hydrodynamic interactions. The particle interaction is modeled via a screened Coulomb potential together with a steric repulsion. A strong electric field leads to lane formation of oppositely driven lanes. Each lane comprises particles of the same charge. A nonequilibrium "phase diagram" classifying different steady states is obtained as a function of the colloidal volume fraction and the Coulomb coupling. Different steady states are characterized by structural correlations perpendicular and parallel to the applied field. We find a variety of different phases involving lane chains at small volume fraction and low screening, and lanes with two-dimensional crystalline order perpendicular to the field at high volume fraction. The lateral crystalline order can be a square, triangular, or rhombic lattice. In between there is a lateral network structure. These predictions can be verified in real-space experiments on oppositely charged colloids.

I. INTRODUCTION

Colloidal suspensions in external fields are excellent model systems to study phase transitions in and out of equilibrium [1,2]. One important example, which builds on the basics of electrophoresis and electro-osmosis [3], is to expose charged colloidal particles to an external electric field. A constant electric field leads to a nonequilibrium drift of the particles. If a binary mixture of oppositely driven particles is considered, there is a transition toward formation of lanes at high driving fields and high concentration of particles. Each lane consists of particles driven alike. This transition was found in Brownian dynamics simulations [4–9] of a binary mixture of repulsive particles driven by opposite forces. It occurs in two and three spatial dimensions, and seems to be a first-order nonequilibrium transition with a hysteresis in a suitable order parameter [4]. Furthermore, there is a transition from lanes to a jammed configuration [10] at very high particle concentrations. The general scenario is reminiscent of that of pedestrians moving in two opposite directions in a pedestrian zone [11,12]. Similar patterns were observed in simulations of granular systems [13,14], at fluid-fluid interfaces [15], in sheared bilayers [16], and in driven diffusive lattice gases [17].

Recently, the formation of lanes was confirmed in real-space experiments by Leunissen *et al.* [18]. The dynamics of oppositely charged colloidal suspensions in an external field was studied by confocal microscopy. In the absence of an electric driving field, these suspensions form binary crystals [19,20] coexisting with a vacuum. If the applied field strength exceeds a critical threshold, the equilibrium crystal is destroyed and particles form lanes parallel to the applied field, or jam in opposing bands perpendicular to the field direction.

In this paper, we study a simple model designed for the experimental situation of Ref. [18]. A binary mixture of oppositely charged hard-core colloids is considered, which are interacting via a screened Coulomb (or Yukawa) potential. The particles are subjected to an external electric field which drives the system out of equilibrium. The particles perform Brownian dynamics. In order to keep the model as simple as possible, hydrodynamic interactions mediated by the solvent flow are ignored.

A nonequilibrium steady-state diagram is obtained as a function of the colloidal volume fraction and the Coulomb screening. Different steady states are characterized by structural correlations perpendicular and parallel to the applied field. As a result we find a variety of different phases. First, a situation without any macroscopic lanes occurs, which is well separated from another one with lane formation. The latter state can be a chain of lanes at small volume fraction and low screening. At high volume fraction, on the other hand, lanes with two-dimensional crystalline order perpendicular to the field are found. Different lateral crystalline structures involving squares, triangles, and rhombic cells are stable. Furthermore, lanes with a phase-separating fluidlike network structure in the lateral dimension do exist for intermediate volume fractions. Our predictions should stimulate further experimental activity. A quantitative comparison with experimental data is in progress and will be presented elsewhere.

The paper is organized as follows. In Sec. II, we describe our model. In Sec. III, we define order parameters and structural correlations, which we utilize to characterize different states. Brownian dynamics simulation results are presented in Sec. IV. We conclude in Sec. V.

II. THE MODEL

We consider an equimolar binary mixture of $N_A = N_B = N/2$ oppositely charged colloidal particles in three spatial dimensions, where A and B label the two different species. The particles interact via an effective screened Coulomb potential (or Yukawa potential) plus a steric repulsion V_h:
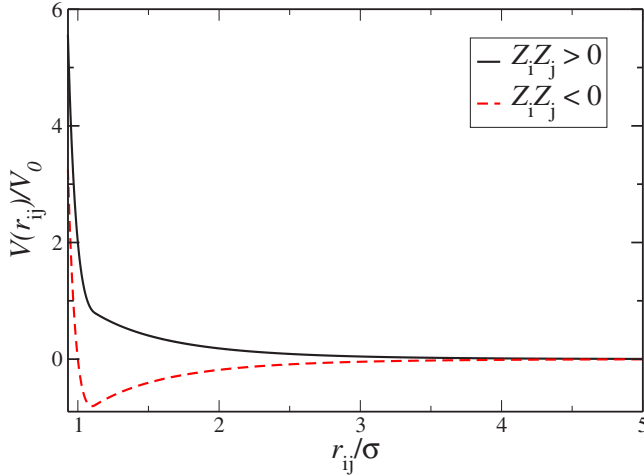
FIG. 1. (Color online) Interaction potential between like-charged (solid) and oppositely charged (dashed) particles for $\kappa\sigma = 1$ and $\sigma_{LJ} \equiv \sigma$.

$$V(r_{ij}) = Z_i Z_j \frac{V_0}{(1 + \kappa\sigma/2)^2} \frac{e^{[-\kappa\sigma(r_{ij}/\sigma - 1)]}}{r_{ij}/\sigma} + V_h(r_{ij}). \quad (1)$$

It has been shown experimentally that this Yukawa interaction is a suitable effective interaction for this system [18,21]. Here, V_0 is the strength of the potential and σ is the particle diameter, which serves as a length scale henceforth. Z_i and $\mathbf{r}_i$ denote the charge and the position of particle i, respectively. $r_{ij} = |\mathbf{r}_i - \mathbf{r}_j|$ is the distance between particles i and j, $i, j = 1, \ldots, N$. The charges of the particles are chosen to be equal in absolute values, i.e., $Z_A = -Z_B = |Z|$. The inverse screening length κ governs the range of the interaction and can be tuned, e.g., by the salt concentration of the solution. The steric repulsion between the particles, which prevents the system from collapsing, is approximated by a shifted and truncated Lennard-Jones potential

$$V_h(r_{ij}) = \begin{cases} \epsilon\left[\left(\dfrac{\sigma_{LJ}}{r_{ij}}\right)^{12} - \left(\dfrac{\sigma_{LJ}}{r_{ij}}\right)^6 + \dfrac{1}{4}\right] & \text{if } r_{ij} \leq 2^{1/6}\sigma_{LJ}, \\ 0 & \text{else}, \end{cases}$$
$$(2)$$

with $\epsilon = 4|Z|^2 V_0/(1 + \kappa\sigma/2)^2$. σ_{LJ} is the effective Lennard-Jones diameter. In our studies we chose $\sigma_{LJ} \equiv \sigma$. A plot of the potential is shown in Fig. 1. The particles move in a fluid of viscosity η and the system is held at fixed temperature T.

The dynamics are supposed to be completely overdamped Brownian motion and we ignore hydrodynamic interactions. The equations of motion for the particles' trajectories $\mathbf{r}_i(t)$, $i = 1, \ldots, N$, are then the stochastic Langevin equations given by [22]

$$\frac{d\mathbf{r}_i(t)}{dt} = \frac{1}{\gamma}\left(\sum_{j=1}^{N} -\nabla_{\mathbf{r}_i} V(r_{ij}) + \mathbf{F}_i^{\text{ext}}(\mathbf{r}_i)\right) + \mathbf{r}_i^R(t). \quad (3)$$

In Eq. (3) above, $\gamma = 3\pi\eta\sigma$ is the friction coefficient. $\mathbf{F}_i^{\text{ext}}$ is the external force acting on the particle i. In our studies presented here, we consider a constant external electric driving field

$$\mathbf{F}_i^{\text{ext}} = Z_i f \mathbf{e}_z, \quad (4)$$

where $\mathbf{e}_z$ is the unit vector along the z direction and f is the strength of the external electric field. Since the colloidal particles are oppositely charged, the external field drives the different species in opposite directions. $\mathbf{r}_i^R(t)$ denotes the random displacement due to the kicks of the solvent molecules acting on the colloidal particles. In Brownian dynamics simulation algorithms, where time evolution is deemed to occur in time steps of fixed length Δt, the finite random displacements $\mathbf{r}_i^R(t)$ are chosen from a Gaussian distribution having the properties [22]

$$\langle \Delta\mathbf{r}_i^R(t)\rangle_G = 0, \quad (5)$$

$$\langle \Delta\mathbf{r}_i^R(t)\Delta\mathbf{r}_j^R(t')\rangle_G = 2D\mathbf{I}\delta_{ij}\delta(t - t'), \quad (6)$$

where $\langle\cdots\rangle_G$ denotes the average over the Gaussian noise distribution, $\mathbf{I}$ is the 3×3 unit matrix, and δ_{ij} denotes Kronecker's symbol. D is the Stokes-Einstein diffusion coefficient, for which the Einstein relation gives $\gamma D = k_B T$, where $k_B T$ is the thermal energy of the system. The integration of Eq. (3) is carried out by using the stochastic Runge-Kutta algorithm which has been shown [23,24] to give more accurate results than the conventional Brownian dynamics algorithm of Ermak [25].

Our model is specified by different input parameters such as the volume fraction $\phi = \pi\rho\sigma^3/6$ of the colloidal particles, with $\rho = N/\Omega$ the number density and Ω the system's volume, the dimensionless inverse screening length $\kappa^* = \kappa\sigma$, and the dimensionless ratios $U_0 = Z^2 V_0/k_B T$ and $f^* = |Z|f\sigma/k_B T$. The parameters chosen correspond to the experimental situation of Ref. [18]. In our studies we keep $U_0 = 50$ and $f^* = 276$ fixed and vary the inverse screening length and the volume fraction. We chose a strong field to ensure that we are in the laning regime. In addition to the length scale σ, a suitable time scale is $\tau_B = \gamma\sigma^2$. The Langevin equations of motion including the external field are numerically solved using a finite time step $\Delta t = 0.00005\tau_B$ in all simulations. We use a cubic box with periodic boundary conditions in all three directions. The number of particles in the cubic simulation box of length L is $N_A = N_B = 1000$. The length L is adjusted such that $\phi = N\pi\sigma^3/6L^3$. We tried different starting configurations but the system was observed to run into the same nonequilibrium steady state independent of the initial configuration, unless stated differently in the text. Statistics were gathered after an initial relaxation period of $20\tau_B$. We address the issue of system-size effects in Sec. IV C.

III. ORDER PARAMETERS AND STRUCTURAL CORRELATIONS

We monitor a suitable order parameter Φ to detect the laning transition, which is defined as follows. An order parameter $\Phi_i = (n_l - n_o)^2/(n_l + n_o)^2$ is assigned to every particle i.
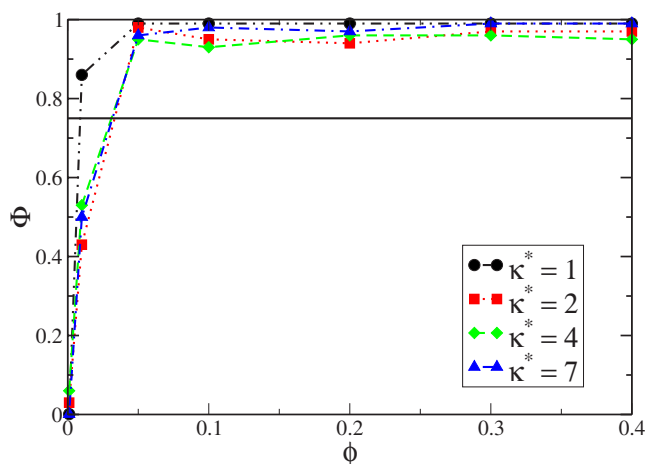
FIG. 2. (Color online) Dimensionless order parameter Φ as a function of the volume fraction ϕ for different inverse screening lengths κ^*. The straight line indicates the threshold dividing states of lanes (above) from states of no lanes (below).

The numbers n_l and n_o are the numbers of like-charged particles and oppositely charged particles, respectively, whose projections of distance onto the plane perpendicular to the field are smaller than a suitable cutoff length scale z_c. This order parameter is equal to 1 if all particles within this distance criterion are of the same kind and zero if $n_l = n_o$, i.e., a homogeneous mixture. We chose for convenience $z_c = \frac{3}{4}\sigma$ to detect all lanes starting from a single queue of particles. The global order parameter Φ is then defined as

$$\Phi = \frac{1}{N}\left\langle \sum_{i=1}^{N} \Phi_i \right\rangle_t, \qquad (7)$$

where the angular brackets $\langle \cdots \rangle_t$ denote a time average. The global order parameter Φ is practically zero for a homogeneous mixed configuration, since oppositely charged particles will be found inside the cutoff distance but it gets close to unity if the same particles are located on top of each other, i.e., in a state of lanes. In what follows we will use the following threshold: for $\Phi \geq 3/4$ we call the configuration a state of lanes while in the opposite case $(\Phi < 3/4)$ we call it a state without lanes. A typical result for the order parameter Φ as a function of the volume fraction ϕ is depicted in Fig. 2 for different inverse screening lengths κ^*. We observe that for low volume fractions $\phi < 0.01$ the laning order parameter is small, but upon increasing the volume fraction it sharply increases to a value close to unity. Only for strongly Coulomb coupled particles, $\kappa^* \lesssim 1$, is the order parameter in the laning regime for $\phi = 0.01$. This behavior can be understood intuitively. When the volume fraction and the Coulomb coupling are small, the mean particle separation is several diameters and thus the particles are hardly correlated and do not form lanes; whereas for sufficiently high densities or sufficiently low κ^* we observe lane formation due to the stronger interaction.

As mentioned in the Introduction we find a variety of different situations within the laning regime depending on the volume fraction and the screening length. Therefore, we monitor the following analysis tools to classify different states of lanes. We calculate a pair distribution function perpendicular to the field direction to check for the structure in the lateral direction which is defined as follows:

$$g_\perp(r_\perp) = \frac{1}{\rho N}\left\langle \sum_{\substack{i,j \\ (i \neq j)}}^{N} \delta(\mathbf{r}_\perp - |\mathbf{r}_{i\perp} - \mathbf{r}_{j\perp}|)\delta(z_i - z_j) \right\rangle_t. \qquad (8)$$

Here, $\mathbf{r}_\perp$ denotes the lateral direction, i.e., $\mathbf{r} = (\mathbf{r}_\perp, z)$. Similarly, we calculate the pair distribution functions between the different particle species $g_{AB}(r_\perp)$ and like-charged particles $g_{AA}(r_\perp)$, which are defined as follows:

$$g_{AB}(r_\perp) = \frac{2}{\rho N}\left\langle \sum_{\substack{i,j \\ (z_i \neq z_j)}}^{N} \delta(\mathbf{r}_\perp - |\mathbf{r}_{i\perp} - \mathbf{r}_{j\perp}|)\delta(z_i - z_j) \right\rangle_t \qquad (9)$$

and

$$g_{AA}(r_\perp) = \frac{2}{\rho N}\left\langle \sum_{\substack{i,j \\ (z_i = z_j, i \neq j)}}^{N} \delta(\mathbf{r}_\perp - |\mathbf{r}_{i\perp} - \mathbf{r}_{j\perp}|)\delta(z_i - z_j) \right\rangle_t. \qquad (10)$$

Additionally, we calculate the Fourier transforms $\hat{h}_X(k)$ of $h_X(r_\perp) = g_X(r_\perp) - 1$ to obtain the structure factors

$$S_X(k) = 1 + \rho \hat{h}_X(k), \qquad (11)$$

with $X = \perp, AA, AB$ and the wave vector $k = |\mathbf{k}|$, where $\mathbf{k} = (2\pi/L)(k_x, k_y)$ and k_x and k_y are integers. A prepeak in the structure factor is an indication of an additional mesoscopic length scale as is typical for bicontinous networks, such as, e.g., microemulsions [26,27].

To detect two-dimensional crystallization in the lateral direction we monitor bond-order parameters $\langle \Psi^{(k)} \rangle$ similar to those frequently used in two-dimensional systems [28–31]. These order parameters check for symmetry of the bonds between particles. We assign to every particle a local bond-order parameter

$$\Psi_i^{(k)} = \left| \frac{1}{N_b}\sum_{j=1}^{N_b} e^{ki\Theta_{ij}} \right|, \qquad (12)$$

which is close to unity for a particle whose neighbors have a k-fold symmetry, and remains small otherwise. The global bond-order parameters $\langle \Psi^{(k)} \rangle$ are then defined by

$$\langle \Psi^{(k)} \rangle = \frac{1}{N}\left\langle \sum_{i=1}^{N} \Psi_i^{(k)} \right\rangle_t. \qquad (13)$$

In Eq. (13), i runs over all particles of the system, and in Eq. (12), j runs over all neighbors of i, Θ_{ij} denotes the angle between the projection of the bond connecting particles i and j onto the xy plane and an arbitrary but fixed reference axis in this plane, and N_b denotes the number of bonds of particle i. We define a bond between two particles if they are next neighbors in the z direction and their projected distance onto the xy plane is less than 1.3σ and more than σ. This some-
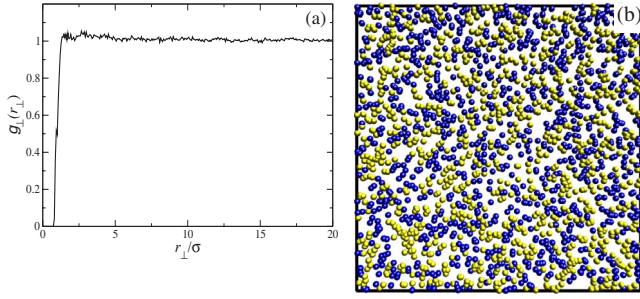
FIG. 3. (Color online) Pair distribution function $g_\perp(r_\perp)$ as defined in Eq. (8) for $\phi=0.01$ and $\kappa^*=7$ (a) and the corresponding projections of the particle positions onto the area perpendicular to the field (b).

what arbitrary definition may be applied since we find that the resulting $\Psi^{(k)}$ depends only weakly on the precise definition of the neighbor distance. In fact, it has already been observed earlier that details of the neighborhood definition have negligible influence on the results of the bond-order parameter [29,30]. This allows us to discriminate between a fluidlike structure where all $\langle\Psi^{(k)}\rangle$ are small and a crystalline one. Furthermore, a k-fold symmetry within a crystalline structure in the lateral direction can clearly be detected. The distribution function $P(\Psi_i^{(k)})$ according to Eq. (13) of the local bond-order parameter $\Psi_i^{(k)}$ also sheds light on the *coexistence* of a crystalline phase with a second one, since its distribution reveals a two-peak structure in that case. Thus it allows for detection of coexistence regimes.

IV. RESULTS

A. Different state points

Let us now discuss eight different typical state points shown in Figs. 3–14 below and then summarize more data in a nonequilibrium state diagram in Fig. 15. For each, we monitor the lateral pair distribution function $g_\perp(r_\perp)$ as defined in Eq. (8) and present the results with a typical particle snapshot projected to a plane perpendicular to the applied driving field. We accompany the results with adequate structural correlations and order parameters. The first parameter set is for low density ($\phi=0.01$) and high screening ($\kappa^*=7$); see Fig. 3. In this case, there is no fully developed lane formation, yet the projected particle snapshots reveal some
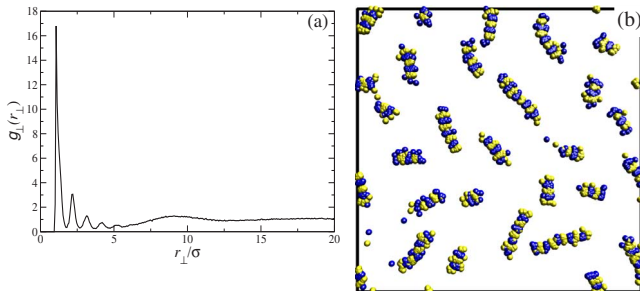

FIG. 4. (Color online) Same as Fig. 3 for $\phi=0.01$ and $\kappa^*=0.2$. Statistics are gathered after an initial relaxation time of $10\tau_B$.
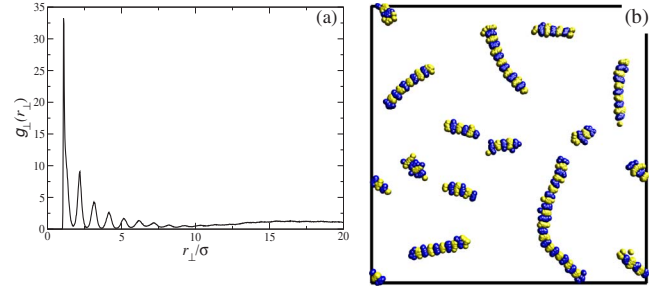

FIG. 5. (Color online) Same as Fig. 4. Statistics are gathered after an initial relaxation time of $320\tau_B$.

anisotropic coarsening which results in an intermediate value of the order parameter $\Phi=0.5$ as shown in Fig. 2. Concomitantly, apart from a correlation hole, there is no liquid or solid structure in the lateral direction, because the particles hardly interact with each other.

The second situation is for low screening and low density ($\phi=0.01$). Then, initially a few lanes of oppositely charged particles form chainlike objects, i.e., a string of alternating lanes; see Fig. 4. This formation process occurs typically within a few τ_B, when starting from a mixed disordered configuration. We emphasize that a strong mutual attraction is needed to stabilize the chains; no chains are obtained for repulsive Yukawa mixtures [4]. It is interesting to follow the further dynamical evolution of the chains. Then, neighboring lane chains fuse subsequently and grow. The fusing process is slow compared to the initial formation of the small chains. The growing process can clearly be deduced from the projected snapshot of Fig. 5(b) and the corresponding lateral pair correlation function Fig. 5(a), which exhibits an ordering phenomena along the chains. In the latter case, the pair correlation reveals more peaks than in the early stage, showing that the average chain length is growing in time. In Fig. 6 the number of chains N_C as a function of time is displayed. One clearly observes the gradual reduction in the number of chains. The inset shows a log-log plot suggesting that the
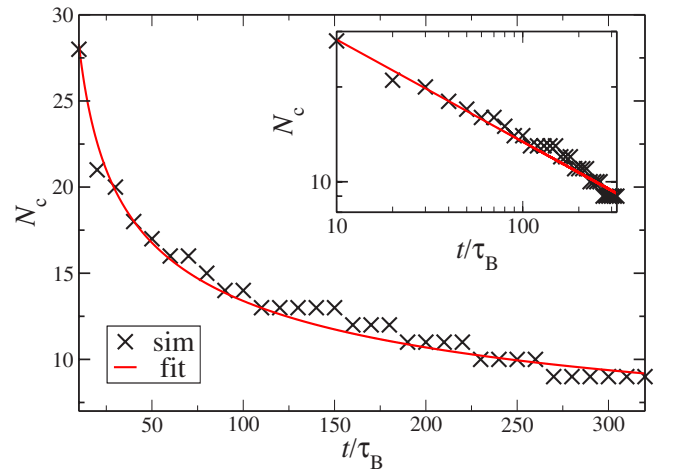

FIG. 6. (Color online) Number of chains N_C as a function of time. The straight line is the best fit of a scaling law to the simulation results (symbols). The inset shows a double-logarithmic plot of the same data.
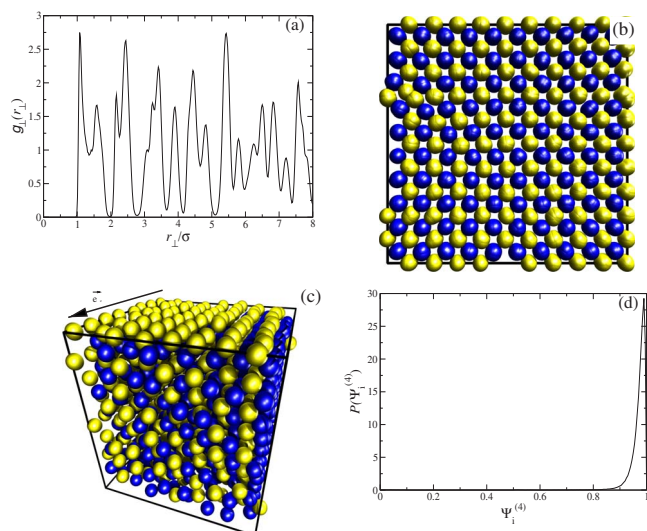
FIG. 7. (Color online) Same as Fig. 3 for $\phi=0.3$ and $\kappa^*=2$. Additionally, a corresponding simulation snapshot (c) and the bond-order parameter distribution $P(\Psi_i^{(4)})$ (d) are shown. The latter clearly indicates a square lattice in the lateral direction.
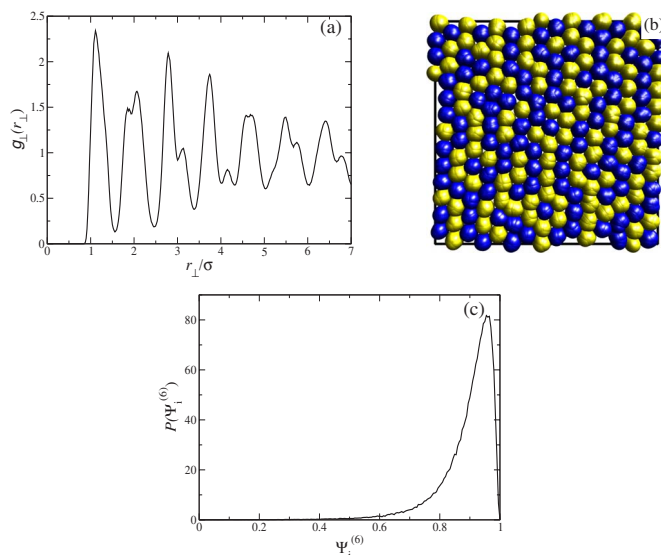

FIG. 8. (Color online) Same as Fig. 3 for $\phi=0.4$ and $\kappa^*=8$. Additionally, the bond-order parameter distribution $P(\Psi_i^{(6)})$ (c) is shown. It clearly reveals a sixfold symmetry of the lattice in the lateral direction.

decrease follows a scaling law with best fit $N_C=A/t^\alpha$ with $A=60$ and $\alpha=0.32$. But, due to the limited time window accessible in the simulation, the ultimate steady state is not clear; one may conjecture that it is a fully phase-separated region coexisting with a region of no lanes. Nevertheless, the lane chains should be clearly observable as transient dynamical states in an experiment. A similar chain formation is observed for higher volume fraction up to $\phi=0.05$. The appearance of chains can be qualitatively understood when regarding pairs of lanes. Since a lane pair of oppositely charged particles clearly possesses a dipolar moment the effective interaction between pairs is expected to be like that between dipoles. In fact, a similar chaining behavior has also been observed in equilibrium dipolar fluids; see, e.g., [32–34].

Next we explore a parameter combination with low screening and high density; see Fig. 7, where data for $\phi=0.3$ and $\kappa^*=2$ are shown. As is clearly visible from both the pair correlation function and the projected snapshots, a lateral crystal-like order emerges. Oppositely driven lanes are placed on a square lattice as the high value of $\langle\Psi^{(4)}\rangle=0.95$ clearly reveals. The sharp distribution of $P(\Psi_i^{(4)})$ depicted in Fig. 7(d) indicates indeed a single state with fourfold symmetry. This lattice formation can be qualitatively understood from an effective interaction between oppositely charged driven lanes which has a short-ranged repulsive part and a long-ranged attractive interaction. The former is caused by friction between oppositely driven particles, while the latter just results from the bare Coulomb interaction. From the data we conclude that the positional order in the lane location is really long ranged. This is supported by a simulation of a system that is eight times bigger, as will be discussed in Sec. IV C.

The next parameter combination is high screening and high volume fraction, $\phi=0.4$ and $\kappa^*=8$; see Fig. 8. Here the strong friction between oppositely driven particles enforces

lane formation, and the high density results in a rhombic or triangular packing of different lanes. This lattice is then decorated with different charges. The sixfold symmetry of the lattice of this parameter combination is revealed by the averaged value of $\langle\Psi^{(6)}\rangle=0.83$. The distribution of $\Psi_i^{(6)}$ is also shown in Fig. 8(c). For less screening, $\kappa^*\lesssim3$, we find a rhombic lattice with a twofold symmetry.

Next we go for further intermediate cases. The most striking new state occurs at high screening and intermediate volume fraction; see Figs. 9 and 10, where data for $\phi=0.1$ and $\kappa^*=5$ and 10 are shown. Here one encounters an in-plane structure reminiscent of a percolating network, bicontinuous microemulsion, or microphase-separated system. We call this structure networklike. It is characterized by liquidlike order in the lateral direction [see Figs. 9(a) and 10(a)]. The prepeaks in the structure factors $S_{AA}(k)$ in Fig. 11(b) reveal an additional length scale that depends on the screening length κ^*. The peaks clearly show that the average thickness of the lateral regions of like-charged particles is significantly affected by the choice of κ^*. The characteristic spacing in this structure can be also extracted from the pair correlation function between the different particle species g_{AB} as defined in Eq. (9) [see Fig. 11(a)]. These result show that the char-
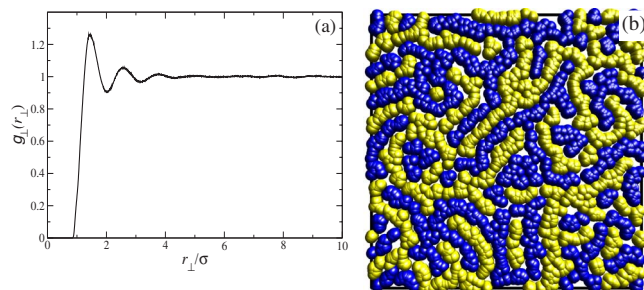

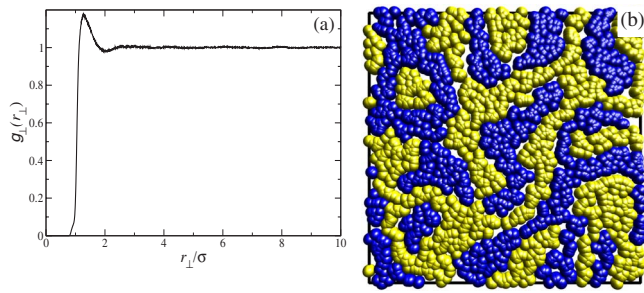FIG. 9. (Color online) Same as Fig. 3 for $\phi=0.1$ and $\kappa^*=5$.

FIG. 10. (Color online) Same as Fig. 3 for $\phi=0.1$ and $\kappa^*=10$.

acteristic spacing is increasing with increasing κ^*. This is also qualitatively supported from the projection snapshots in Figs. 9(b) and 10(b).

Then we observed a mixed situation of two coexisting dynamical states. Coexisting states are characterized by two peaks in the appropriate bond-order parameter distribution, indicating that parts of the system are in a k-fold regime
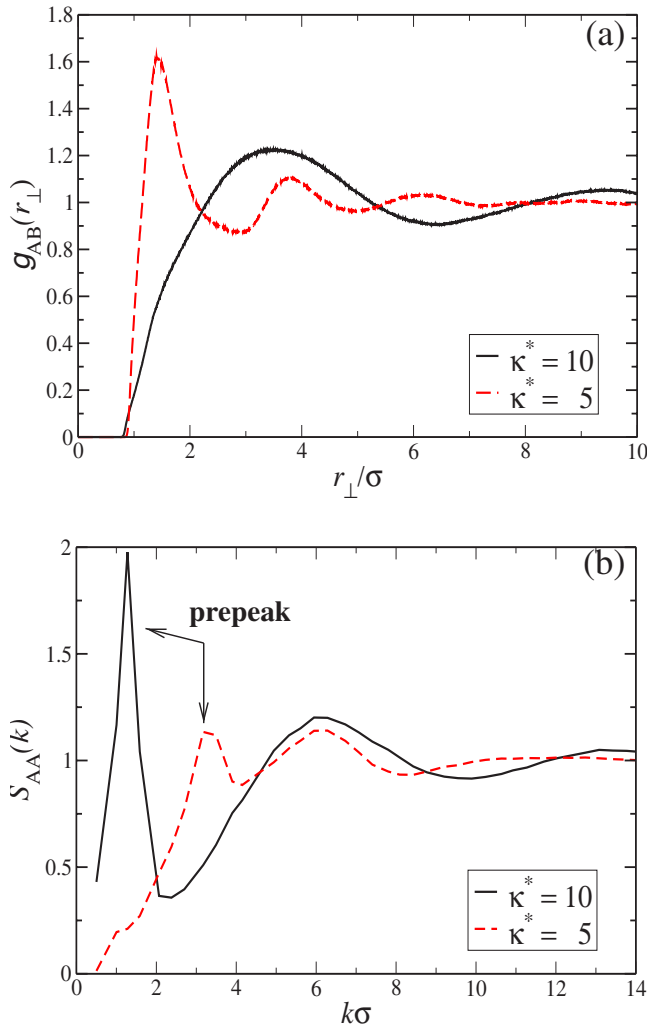

FIG. 11. (Color online) Pair distribution function $g_{AB}(\mathbf{r}_\perp)$ (a) and structure factor $S_{AA}(k)$ of like-charged particles (b) for $\phi=0.1$ and $\kappa^*=5$ and 10.
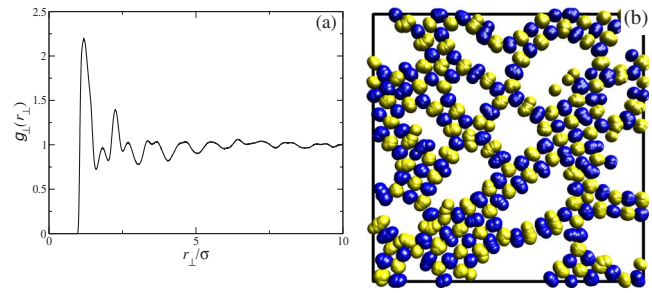

FIG. 12. (Color online) Same as Fig. 3 for $\phi=0.1$ and $\kappa^*=1$.

while other parts of the system are not. These results are summarized in Figs. 12 and 14. The former shows a coexistence between a region of no lanes and a square lattice phase which involves empty holes and the fourfold symmetry in the lattice is indicated by the second peak in the bond-order parameter distribution both depicted in Fig. 13(a). The pre-peak in the structure factor $S_\perp(k)$ in Fig. 13(b) shows an additional length scale caused by the voids. But, as in the chaining situation, it is not completely clear whether this is a transient state toward a complete square lattice and no lanes phase separation, or whether this is a stable state. However, if a completely separated state is used as a different starting configuration, it stays stable well over the time explored by the simulation.

Finally in the projected snapshot of Fig. 14(b) one observes both local network structures and parts with triangular
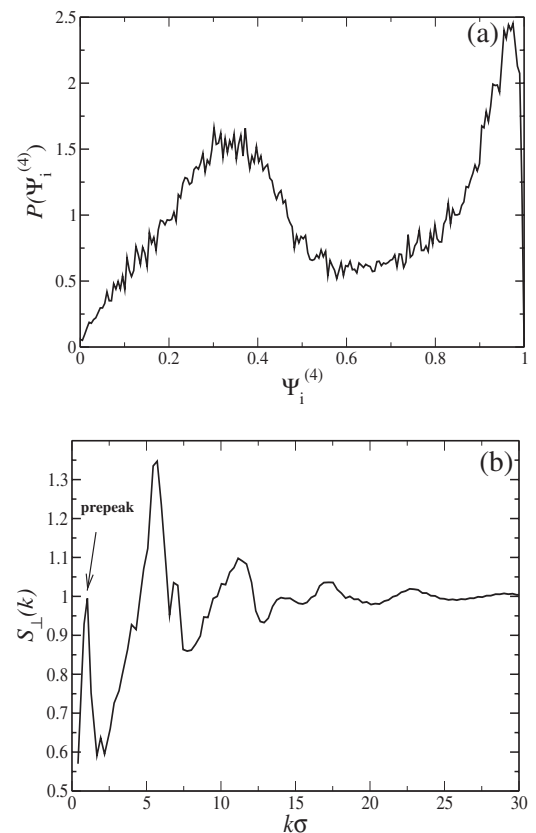

FIG. 13. Bond-order parameter distribution $P(\psi_i^{(4)})$ (a) and structure factor $S_\perp(k)$ (b) for $\phi=0.1$ and $\kappa^*=1$.
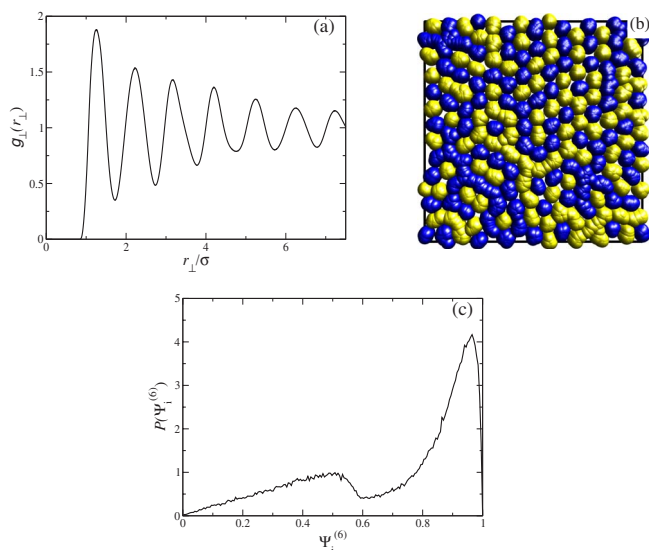
FIG. 14. (Color online) Same as Fig. 3 for $\phi=0.3$ and $\kappa^*=7$. Additionally, the bond-order parameter distribution $P(\Psi_i^{(6)})$ (c) is shown. It clearly reveals that parts of the system are in a sixfold symmetry while others are not.

crystallinity. The underlying sixfold symmetry is again revealed by the bond-order parameter distribution.

B. Steady-state phase diagram

In Fig. 15 we present a nonequilibrium steady-state phase diagram for fixed driving force as a function of the screening parameter κ^* and the volume fraction ϕ. In addition to the eight parameter combinations that were already discussed in detail, more data are collected here. There are stable states with no lanes, network-forming lanes, square, triangular, and rhombic lateral crystals of lanes, and associated coexistence situations. Solid lines separate the different states. The chain formation is shown as well. The broken line separating this state from the others indicates that we are not sure whether this is a transient state on the way to square and no-lane
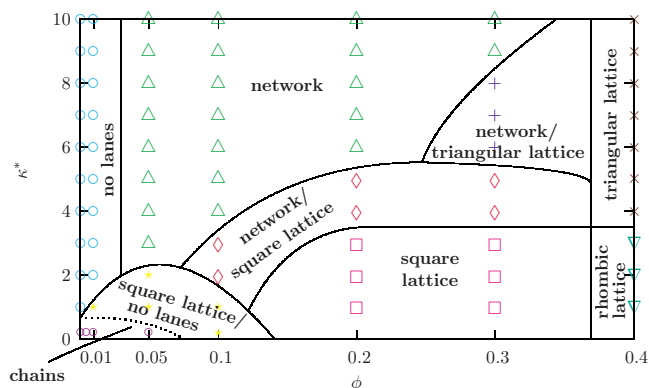

FIG. 15. (Color online) Nonequilibrium steady-state phase diagram for a constant driving force of strength $f^*=236$. All different states described in Figs. 3–14 are displayed in the plane perpendicular to the external fields as a function of the inverse screening length κ^* and the volume fraction ϕ. The lines are a guide for the eye.

coexistence or a stable state. This phase diagram should be detectable in experiments on highly charged colloidal suspensions.

It is interesting to correlate our results with in equilibrium the phase diagram of the same system in equilibrium without an external field which was calculated by Hynninen *et al.* for $\kappa^*=6$ and varying temperatures and volume fractions in [19]. Similar to our results, they find a variety of different stable states due to the competition between the repulsive core and the screened Coulombic attraction. Let us first go through the phase diagrams from low to high volume fractions for weak Coulomb coupling, which corresponds to high temperature in the phase diagram of Hynninen *et al.* and high screening in ours. In equilibrium one encounters first a fluid phase, then a fluid and fcc-disordered coexistence regime, and ends up in a fcc-disordered phase. Analogously, in our phase diagram we start from two regimes with no crystalline order, namely, no lanes and network, and go through a triangular lattice–network coexistence to a triangular lattice. This part of the phase diagram is in both cases mainly dominated by the repulsive core. For stronger Coulomb coupling, on the other hand, the equilibrium case reveals a broad gas-CsCl coexistence. The corresponding part in our phase diagram shows similarly a coexistence between a square lattice and no lanes. In our case we find additionally the special case of coexistence between a square lattice and no lanes: the chain regime. Finally, for higher packing fractions and strongly interacting particles, Hynninen *et al.* find three different crystal structures for increasing volume fractions: CuCl, CsCl, or tetragonal structure. In our case, we find analogously a transition from a square to a rhombic lattice. We emphasize, however, that this is just a qualitative comparison between an equilibrium and a nonequilibrium phase diagram.

C. Finite system size effects

We have also addressed the issue whether the observed results are influenced by the system size and whether the periodic boundary conditions support lane formation. Therefore, we carried out several benchmark simulations with a system that is eight times bigger, i.e., $N=16\,000$ particles. We applied the same external field as previously as well as a field tilted by 45° such that lanes do not connect themselves due to the periodic boundary conditions. We compare the simulations to the previous results after the same initial simulation time. We find that the qualitative results are influenced neither by system size nor by the field direction. We further confirm that the quantitative results depend only weakly on the system size.

We exemplify this with two state points and compare them to earlier discussed results. First, we consider $\phi=0.01$ and $\kappa^*=0.2$. For this parameter combination we find chains of lanes. Typical projections of the particles' positions onto the area perpendicular to the field for $N=2000$ and $16\,000$ are presented in Fig. 16. For the larger system only $1/8$ of the system is displayed to enable comparison on the same dimensions. Obviously, we find qualitative agreement with the previously shown results. The quantitative agreement can be deduced from the pair distribution functions $g_\perp(r_\perp)$ in
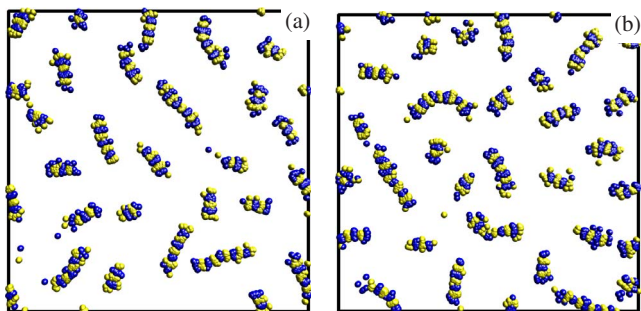
FIG. 16. (Color online) Projections of the particles' positions onto the area perpendicular to the field for $\phi=0.01$ and $\kappa^*=0.2$ after an initial relaxation time of $10\tau_B$. (a) Same plot as in Fig. 4(b). (b) Same setup but for $N=16\,000$ particles. For (b) only $1/8$ of the system is displayed to compare with the smaller system depicted in (a) on the same dimensions.

Fig. 17. They reveal the same number of peaks, suggesting that the average width of a chain is nearly unaltered by the system size.

The second state point is $\phi=0.1$ and $k^*=10$, where we find a networklike structure. In Figs. 18(a) and 18(b) the projected particle positions for the two system sizes with the same driving field are displayed. To make the point, for the larger system we again show only $1/8$ of the system. Once again, the qualitative agreement is obvious. Quantitatively, we compare the pair distribution functions $g_{AB}(r_\perp)$ in Fig. 19. It suggests that the characteristic spacing is more or less system-size independent.

The influence of the periodic boundary conditions, which support laning by connecting the lanes to each other when the driving field is along the box orientation is also small, as can be seen when tilting the external driving field. We then find the same qualitative behavior; see Figs. 18(a) and 18(c). Here, we depict a simulation snapshot for an external field tilted by $45°$, i.e., $\mathbf{E}_i^{ext}=Z_i f(\mathbf{e}_y+\mathbf{e}_z)/\sqrt{2}$.
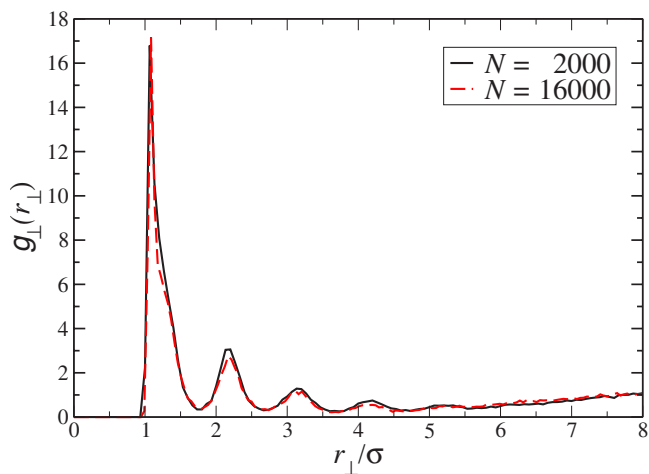

FIG. 17. (Color online) Pair distribution functions $g_\perp(r_\perp)$ for $\phi=0.01$ and $k^*=0.2$ for two different system sizes $N=2000$ and 16 000 after an initial relaxation time of $10\tau_B$.
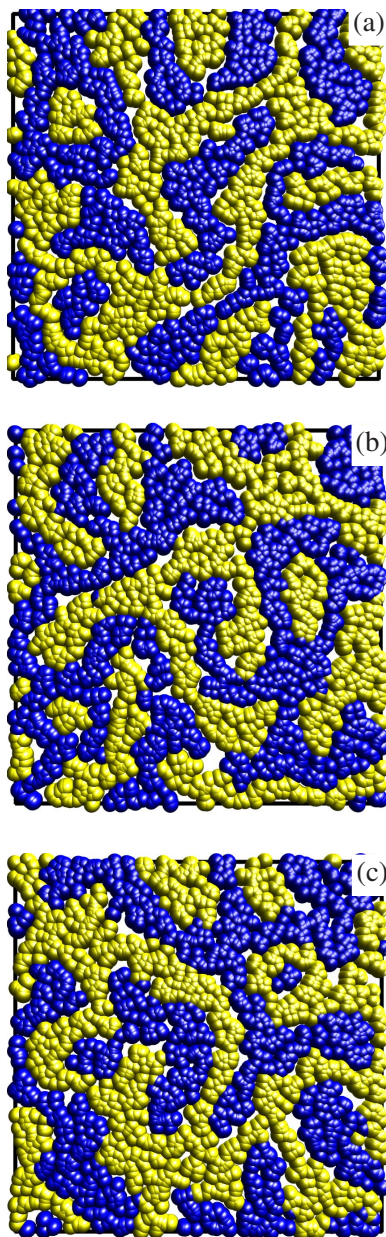
FIG. 18. (Color online) Projections of the particles' positions onto the area perpendicular to the field for $\phi=0.1$ and $\kappa^*=10$. (a) Same plot as in Fig. 10(b). (b), (c) Same setup but for $N=16\,000$ particles. In (c) the external driving field is tilted by $45°$ such that the lanes do not connect themselves due to the periodic boundary conditions. For (b) and (c) only $1/8$ of the system is displayed to compare with the smaller system depicted in (a) on the same dimensions.

V. CONCLUSION

In conclusion, we have analyzed steady states in a driven mixture of oppositely charged colloidal particles which exhibit lane formation. By structural diagnostics, different states were distinguished via a different degree and order of the lanes. At high Coulomb coupling and low densities, a chaining of oppositely charged lanes was observed. Furthermore, there is the possibility of lateral crystallization of lanes
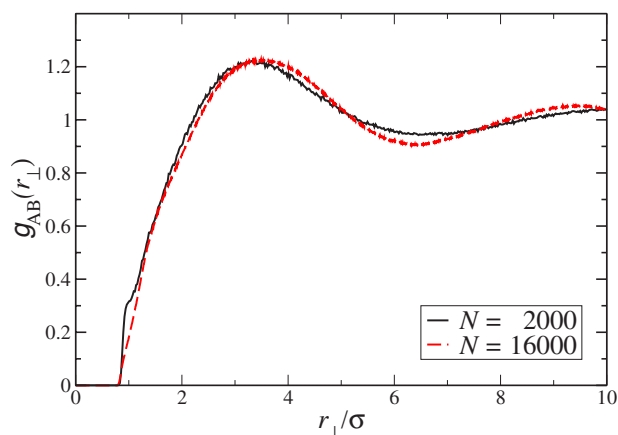
FIG. 19. (Color online) Pair distribution functions $g_{AB}(r_\perp)$ for $\phi=0.1$ and $k^*=10$ for two different system sizes $N=2000$ and 16 000.

into two-dimensional square, triangular, or rhombic lattices. This state occurs for high densities.

In the future we shall focus on a detailed comparison between our simulation data and the experimental data from Ref. [18]. Work along these lines is in progress. It would be interesting to check whether effective dipolar interactions between the charged particles, which are mediated by the distorted counterion cloud around the colloids in an electric field, are relevant. These forces favor aligning particles no matter how they are charged. Furthermore, one should more carefully incorporate and study hydrodynamic interactions between the colloidal particles mediated by the solvent flow [35]. We expect that hydrodynamic interactions disfavor lanes driven in opposite directions next to each other, resulting in a competition between Coulombic and hydrodynamic interactions. However, for strongly charged particles at low physical volume fractions, we expect a minor influence of hydrodynamic interactions such that the topology of the phase diagram can be observed in a real-space experiment.

It would further be interesting to generalize the setup to driven nonspherical particles like rodlike particles and/or to rod-plate mixtures where new effects are anticipated [36–38]. Finally, the special case of a mixture of charged and uncharged particles, as recently studied by simulation in Ref. [39], should receive more attention and should be classified according to our structural criteria.

ACKNOWLEDGMENTS

[1] T. A. Witten, Rev. Mod. Phys. **71**, S367 (1999).

[2] H. Löwen, J. Phys.: Condens. Matter **13**, R415 (2001).

[3] M. Medebach and T. Palberg, J. Chem. Phys. **119**, 3360 (2003).

[4] J. Dzubiella, G. P. Hoffmann, and H. Löwen, Phys. Rev. E **65**, 021402 (2002).

[5] R. R. Netz, Europhys. Lett. **65**, 616 (2003); a corresponding state in two spatial dimensions was already proposed as an alternating stripe pattern.

[6] J. Chakrabarti, J. Dzubiella, and H. Löwen, Europhys. Lett. **61**, 415 (2003).

[7] H. Löwen and J. Dzubiella, Faraday Discuss. **123**, 99 (2003).

[8] J. Delhommelle, Phys. Rev. E **71**, 016705 (2005).

[9] R. B. Pandey, J. F. Gettrust, R. Seyfarth, and L. A. Cueva-Parra, Int. J. Mod. Phys. C **14**, 955 (2003).

[10] J. Chakrabarti, J. Dzubiella, and H. Löwen, Phys. Rev. E **70**, 012401 (2004).

[11] R. Jiang, D. Helbing, P. K. Shuklai, and Q. S. Wu, Physica A **368**, 567 (2006).

[12] R. Kolbl and D. Helbing, New J. Phys. **5**, 48 (2003).

[13] G. C. M. A. Ehrhardt, A. Stephenson, and P. M. Reis, Phys. Rev. E **71**, 041301 (2005).

[14] M. P. Ciamarra, A. Coniglio, and M. Nicodemi, Phys. Rev. Lett. **94**, 188001 (2005).

[15] A. Wysocki and H. Löwen, J. Phys.: Condens. Matter **16**, 7209 (2004).

[16] M. Das, S. Ramaswamy, and G. Ananthakrishna, Europhys. Lett. **60**, 636 (2002).

[17] G. P. Saracco and E. V. Albano, J. Chem. Phys. **118**, 4157 (2003).

[18] M. E. Leunissen, C. G. Christova, A. P. Hynninen, C. P. Royall, A. I. Campbell, A. Imhof, M. Dijkstra, R. van Roij, and A. van Blaaderen, Nature (London) **437**, 235 (2005).

[19] A. P. Hynninen, M. E. Leunissen, A. van Blaaderen, and M. Dijkstra, Phys. Rev. Lett. **96**, 018303 (2006).

[20] A. P. Hynninen, C. G. Christova, R. van Roij, A. van Blaaderen, and M. Dijkstra, Phys. Rev. Lett. **96**, 138308 (2006).

[21] C. P. Royall, M. E. Leunissen, A. P. Hynninen, M. Dijkstra, and A. van Blaaderen, J. Chem. Phys. **124**, 244706 (2006).

[22] *Computer Simulation of Liquids*, edited by M. P. Allen and D. J. Tildesley (Clarendon Press, Oxford, 1989).

[23] A. C. Brańka and D. M. Heyes, Mol. Phys. **98**, 1949 (2000).

[24] A. C. Brańka and D. M. Heyes, Phys. Rev. E **60**, 2381 (1999).

[25] D. L. Ermak, J. Chem. Phys. **62**, 4189 (1975).

[26] M. Teubner and R. Strey, J. Chem. Phys. **87**, 3195 (1987).

[27] G. Gompper and M. Schick, Phys. Rev. Lett. **62**, 1647 (1989).

[28] A. Jaster, Europhys. Lett. **42**, 277 (1998).

[29] H. Weber, D. Marx, and K. Binder, Phys. Rev. B **51**, 14636 (1995).

[30] M. Heni and H. Löwen, J. Phys.: Condens. Matter **13**, 4675 (2001).

[31] B. I. Halperin and D. R. Nelson, Phys. Rev. Lett. **41**, 121 (1978).

[32] T. Tlusty and S. A. Safran, Nature (London) **290**, 1328 (2000).

[33] J. J. Weis, J. Phys.: Condens. Matter **15**, S1471 (2003).

[34] J. J. Weis, J. M. Tavares, and M. M. T. da Gama, J. Phys.:

Condens. Matter **14**, 9171 (2002).

[35] D. Long and A. Ajdari, Eur. Phys. J. E **4**, 29 (2001).

[36] R. Kirchhoff and H. Löwen, Europhys. Lett. **69**, 291 (2005).

[37] R. Kirchhoff and H. Löwen, J. Phys.: Condens. Matter **17**, 7805 (2005).

[38] H. H. Wensink and H. Löwen, Phys. Rev. Lett. **97**, 038303 (2006).

[39] C. Reichhardt and C. J. Olson Reichhardt, Phys. Rev. E **74**, 011403 (2006).